Numerical Investigations of Detonation Reinitiation and Failure Modes from Mach Reflection

Shiyan Zhang[a], Shuyue Lai[b,*], Shizhi Tang[b], LinLin Yang[c], Fei Qi[b], Xiaohang Fang[d]

[a] *School of Aeronautics and Astronautics, Shanghai Jiao Tong University (SJTU), Shanghai, China*
[b] *School of Mechanical Engineering, Shanghai Jiao Tong University (SJTU), Shanghai, China*
[c] *Department of Engineering Science, University of Oxford, Oxford OX1 3PJ, UK*
[d] *Department of Mechanical & Manufacturing Engineering, University of Calgary, T2L 1Y6, Calgary, Canada*

Abstract

This work demonstrates numerical investigations of stoichiometric hydrogen-air detonation ignition behaviors following a Mach reflection of two incident shocks. Compressible Navier-Stokes equations for two-dimensional reactive flow are solved via a high order numerical algorithm and the chemical reaction follows a calibrated chemical-diffusive model (CDM). A diamond-shaped obstacle is placed at the middle of the channel, creating a converging-diverging cross section, where the detonation waves go through an overdriven-diffraction process. With different converging angles, a Mach reflection of the incident shocks is captured at the trailing edge of the obstacle, accompanied by three distinct detonation propagation modes: detonation reinitiation mode characterized by the transverse detonation waves, shock-flame decoupling mode, and fully quenched mode characterized by an inert shock with no ignition, all of which correspond well with earlier experimental findings. In order to fundamentally understand the reason behind these distinct detonation propagation behaviors and to uncover the critical conditions for detonation reinitiation, two theoretical approaches, including the $D(\kappa)$ curve from the generalized ZND model based on the weakly-curved quasi-steady detonation by Kasimov and Stewart, as well as the critical decay rate model by Eckett et al. are adopted. The results show that the $D(\kappa)$ curve from ZND model provides a reliable indicator for identifying the detonation reinitiation region in the velocity-curvature distribution map, while the critical decay rate model effectively distinguishes between ignition and complete quenching. This work presents the first numerical study detailing the early-stage ignition mechanism following a Mach reflection of two incident shocks, supporting the previous experimental studies in confirming hydrogen detonations are in good agreement with the critical curvature predicted by the laminar ZND theory.

Keywords: Detonation wave; Mach reflection; Numerical simulation; Weakly-curved quasi-steady detonation;

* Corressponding Author: *laishuyue@sjtu.edu.cn*

Information for Editors and Reviewers

1) Novelty and Significance Statement

For the first time in numerical simulation, a new obstacle configuration is added to the detonation channel to stably generate Mach reflection of incident shocks. The study is significant in revealing the multiple post-reflection detonation behaviors, providing detailed insights into the early-stage ignition mechanisms that are typically inaccessible in experiments. The simulation results validate both the $D(\kappa)$ theory for a weakly-curved detonation and the critical decay rate model in predicting various detonation propagation modes, suggesting the use of these theoretical models as guidance for the design of hydrogen detonation and quenching industrial applications. In addition, comparison with experimental observations and validation against theoretical models presented in this work further confirm the effectiveness of the calibrated chemical-diffusive model (CDM) for modeling detonation propagation and ignition events in hydrogen-air mixtures.

2) Author Contributions

- S. Zhang: Conceptualization, Investigation, Formal analysis, Data curation, Writing –original draft, Writing - Review & Editing.
- S. Lai: Conceptualization, Methodology, Investigation, Supervision, Writing –review & editing, Funding acquisition.
- S. Tang: Investigation, Data curation, Writing – review & editing.
- L. Yang: Investigation, Writing – review & editing.
- F. Qi: Investigation, Supervision, Writing –review & editing, Funding acquisition.
- X. Fang: Conceptualization, Methodology, Supervision, Investigation, Writing –original draft, Writing –review & editing, Funding acquisition.

1. Introduction

Understanding the formation and propagation mechanisms of cellular detonation is vital for industrial safety concerning advanced energy systems and the design of a more efficient propulsion system. The cellular structure of a detonation wave refers to the formation of alternating high and low pressure zones behind the shock front, which is induced by the transverse wave interactions [1]. At each collision of the transverse waves, the Mach reflection influences the local thermodynamic conditions as well as the chemical kinetics, which play a vital role in determining the propagation mode of the detonation. Therefore, identifying the factors that govern the detonation propagation behavior after Mach reflection is crucial for further understanding of the detonation propagation mechanism.

Various studies have focused on detonation quenching and reinitiation physics by considering shock reflection events under different configurations. When the cylindrical obstacle is used for experimental studies and numerical simulations [2, 3], reinitiation occurs as a result of detonation reflection from the obstacle or the channel boundary wall, where either a regular reflection or a Mach reflection is formed and leads to the reinitiation. For unstable detonations, reinitiation appears not only along the Mach stem, hot spots in the heated unburned reactants may also induce local explosions. Another category of experimental studies employs a concave configuration to explore the detonation reflection in an annular pipe [4, 5]. Depending on the magnitude of the wedge angle, there is a shift from Mach reflection to regular reflection during detonation propagation. In this case, the traditional three-shock theory of planar detonation is no longer applicable. To date, relevant studies on the isolated effect of Mach reflections on detonation propagation are still scarce and necessitate further exploration.

Detonation reinitiation, as a significant phenomenon, has been suggested to have a complex mechanism and is influenced by multiple factors. Different obstacle configurations and channel confinements impact the strength and interactions of shock waves intensively [6, 7]. A set of critical length-scale criteria based on the detonation cell size (λ) has been developed. By adding inert porous filters or artificially setting the reactivity gradients to the channel, the role of the reactivity gradient on detonation reinitiation can be well explored [8, 9]. In addition, various turbulent fluctuations as well as fluid instabilities may also contribute to promoting detonation reinitiation [10]. With all these relevant affecting parameters, there lacks a unified theory predicting the onset, stability, and failure of detonation behaviors in various configurations.

Theoretical analysis offers a fundamental approach for understanding and predicting the detonation behaviors. Derived from a one-dimensional detonation configuration, Kasimov and Stewart proposed a model to predict the detonation velocity (D) and the curvature (κ) of the detonation front using quasi-steady weakly-curved detonation assumption, which means the reaction zone evolves slowly on the particle passage time scale and the shock curvature is small relative to reaction zone thickness, and one-step chemical reaction model [11]. Recently, Zangene et al. [12] further verified this theory in their experimental study on the critical conditions for hydrogen detonation. Their study highlighted the critical curvature was well characterized by laminar ZND theory for weakly-curved detonation for the regular structure of hydrogen detonation. Moreover, the critical decay rate model, first developed by Eckett et al.[13], captures the inherently unsteady and transient ignition process behind the decaying shock. It provides a framework to evaluate the effect of ignition delay time and shock decaying characteristic time, and to predict the ignition or extinction. While the finding is significant, uncovering the highly transient behavior of detonation wave formation near the Mach reflection can be challenging through experimental studies alone which motivated the current study. Numerical simulations, on the other hand, allow high-resolution spatiotemporal data for detailed analysis as well as tuning of the incident shock strength through the adjustment of obstacle angles, enabling systematic investigation of detonation dynamics.

In this study, we use high-fidelity numerical simulations to study the detonation attenuation and reinitiation processes in stoichiometric hydrogen-air mixtures following the Mach reflection of two incident shocks. A diamond-shaped obstacle, inspired by the experimental setup proposed by Zangene et al. [12], is placed in the channel to isolate detonation Mach reflection and to study its direct effects on detonation dynamics in a more controlled way. First, the use of the calibrated chemical diffusive model (CDM) [14] to capture the major detonation reinitiation or failure behaviors is validated. Then, the critical transient behaviors of different detonation propagation modes observed by changing the geometric parameters are detailed. The asymptotic analysis method from Detonation Shock Dynamics (DSD) theory is used to calculate the $D(\kappa)$ curve of the hydrogen mixture, which gives the critical envelop of shock speed and shock front curvature from generalized ZND model. Furthermore, the critical decay rate model is also adopted and comparing with the decay rate of different detonation modes, examining the effectiveness of the theoretical models for hydrogen detonation.

2. Numerical and Physical Models

2.1. Governing Equations

In this study, we solve the two-dimensional (2D) fully compressible Navier-Stokes equations for the unsteady compressible reacting flow [15]. Detailed information on the governing equations can be found in the Appendix.

In this work, a previously calibrated chemical diffusive model (CDM) [15] that follows the first-order Arrhenius equation is used where detailed information is included in the appendix. This CDM model for stoichiometric premixed hydrogen-air mixture, optimized by Lu et al. [14] with additional detonation cell size, accurately reproduces key properties of the laminar flames (e.g. flame speed and thickness) and detonations (e.g. Chapman-Jouguet (CJ) speed, half-reaction thickness, and detonation cell size) in agreement with detailed chemistry and experiments. Various prior studies have confirmed that the CDM model can effectively capture the main features of laminar flames, shock-flame interactions, and detonations [16].

In order to solve the reactive NS equations, a fifth-order WENO numerical algorithm with HLLC fluxes is used for the spatial discretization, and a third-order Runge-Kutta algorithm is used for time advancement. The calculations are performed using a uniform grid of 100 μm, which corresponds to about 3-4 grid points per laminar flame thickness and about 10-20 cells per half-reaction thickness. The detailed grid resolution test is shown in the Appendix. Previous studies have shown that the given grid size can capture the main characteristics of flame acceleration, DDT initiation, and detonation propagation for stoichiometric hydrogen-air mixtures [17].

2.2. Computational Setup

In this study, detonation propagates in an obstructed channel filled with stoichiometric hydrogen-air mixture with the initial conditions of 1 atm pressure and 300K temperature. The input parameters of the hydrogen-air reaction model are calibrated, with a relatively low activation energy selected to simulate the detonation phenomenon of weakly-unstable gas; see Appendix for more details. The computational setup is shown in Fig.1, where the channel height is $H = 0.203$ m, and the total channel length is $L3 = 2.0$ m. A diamond-shaped object is positioned 1 m away from the left boundary, forming two converging-diverging channels that induce and overdriven-diffraction process and generate a sustained Mach reflection downstream [12]. All boundaries are symmetric, and the surface of the obstacle is modeled as a no-slip adiabatic wall. The obstacle angle β at the trailing edge is fixed at 60°, which is chosen to obtain the backward-propagating Mach stem as far as possible after the incident waves collide with each other [18]. The leading edge angle, α, is varied to adjust the incident shock strength and to induce different detonation behaviors. The experimental parameters and the main phenomena are listed in Table 1.

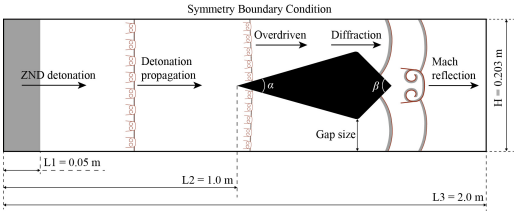

Fig. 1: The schematic of the setup and boundary conditions for the physical model.

Table 1: Geometric parameters for simulation and the corresponding detonation propagation mode.

Case	α [deg]	Gap size [m]	Mode
(i)	10	0.0483	Detonation reinitiation
(ii)	12	0.0393	Detonation reinitiation
(iii)	15	0.0265	Shock flame decouple
(iv)	20	0.0069	Shock no ignition

3. Results and Discussion

In this section, we first present the detonation modes observed in different obstacle configurations. Figure 2 shows the global smoke foils corresponding to three detonation modes, with the x axis ranging from 0.8 to 2.0 m. The detonation forms a relatively stable cellular structure before it reaches the obstacle. Starting from $x = 1.0$ m, the detonation wave is separated into two isolated channels and continuously compressed to an overdriven state. After that, the detonation waves begin to diffract as the channels expand, accompanied by the detonation attenuation and shock flame decoupling to a certain degree. Different detonation modes appear downstream of the obstacle. For case (ii), as a representative of the reinitiation mode, detonation reinitiation first appears on the centerline of the channel, and then gradually develops to the whole channel. When the angle increases to $\alpha = 15^\circ$, the shock front decouples with the flame, and the detonation wave quenches. Further increasing α to 20°, detonation propagates in the form of inert shock without ignition behind the obstacle. The mechanism of each detonation mode will be detailed in later sections.

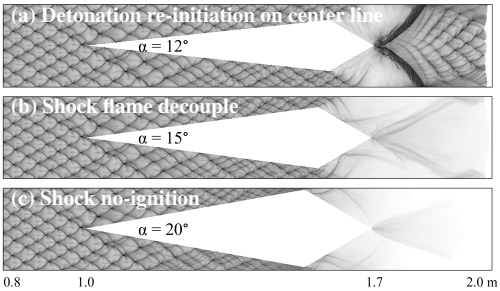

Fig. 2: Global numerical soot foils for different detonation modes. The figure size is 1.2 m $\times$ 0.203 m.

Figure 3 shows the comparisons of local characteristics during Mach reflection between our simulated results and previous experiments [12]. Note that the fuel mixtures used in the current simulation and in the experiment are different ($2H_2/O_2/2Ar$ in the experiment). The key features observed in the three

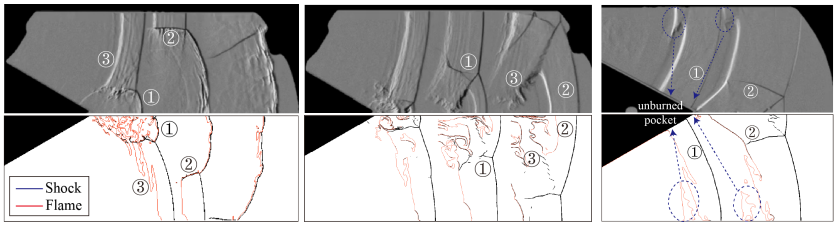

(a) $\alpha = 10°$, detonation reinitiation (b) $\alpha = 15°$, shock flame decouple (c) $\alpha = 20°$, no ignition

Fig. 3: Comparisons of experimental results (upper) [12] and simulation modes (lower). Shocks are represented by iso-surfaces of numerical schlieren, and the flame surface is defined as Y = 0.5.

detonation modes are, however, consistent with each other. For the reinitiation mode, the curved Mach stem (marked as ①) gradually evolves, accomplished by the transverse detonation waves (②) along the induction zone between the shock front and flame surface (③). In Fig.3 (b), flame decouples with the shock front (①) before Mach reflection, and unburned gas accumulates behind the curved Mach stem (②) with the slip line (③) separating the location of flame. For the no-ignition mode in Fig.3 (c), flame lags considerably behind the shock front (①), and leaves the unburned pockets near the boundary wall. After the reflection, the inert Mach stem propagates with the inert transverse shock (②).

3.1. Detonation Reinitiation Mode

Figure 4 shows the temperature fields of detonation reinitiation mode at different instants. It can be seen that in the obstacle expansion region, the flame front decouples from the shock front and forms a series of reaction tongues, indicating the occurrence of detonation attenuation. The first collision of the incident shocks (IS) can be observed at $t = 0.847$ ms, which gives rise to significant increase in local pressure and temperature and then generates the ignition kernel marked as F1 in Fig. 4 (b2). A second collision of the extended incident shocks, which are separated by the reaction tongues, forms the new ignition kernel marked as F2 in the next frame. In Fig. 4 (c-d), the inner ignition kernel F1 induces the local explosion event and consumes the pocket of unburned gas, while the outer ignition kernel F2 forms the triple points of Mach reflection. At $t = 0.861$ ms, the formation of the curved Mach stem can be observed. The transverse wave is divided into two parts at this time: the reactive part connecting with the inner localized explosion, and the inert part from outer Mach reflection. As the Mach stem propagates to the right, the standard transverse detonations are formed at $t = 0.864$ ms, which contain the extended transverse detonation part additionally. This extended wave is an oblique shock wave and reacting slip line that connects the triple point to the transverse detonation wave [19]. These highly transient phenomena at the early-stage of detonation reinitiation, while challenging to capture experimentally, can be clearly resolved here in numerical investigations.

In Fig.4 (f), two apparent transverse detonation waves (TD) move along the induction zone. They are followed by transverse shocks in the flame. The transverse detonations consume almost all the reactants in the induction zone, leaving a non-reactive tail in the vicinity of the triple point. These typical features of this Mach structure are similar to the numerical results from Gamezo et al. [20] and experimental phenomena from Xiao et al. [21]. The generation of this non-reactive tail is a result of the relatively low temperature region between the leading shock and the transverse detonation from double Mach reflection. The structure of the vortex system induced by the Kelvin-Helmholtz instabilities can be observed in the shear layer between the Mach shock region and the transverse waves. As the transverse detonation waves propagate, secondary reflections occur after their collisions with the channel wall. It is also worth noting that compared to hydrocarbon experiments where the reaction front is characterized by significant hydrodynamics fluctuations and unreacted pockets, the reaction fronts seen in our numerical simulations are rather inline with laminar reaction front characteristics. Such differences between hydrogen and other hydrocarbon in detonation wave formation are also highlighted in previous work[12].

3.2. Detonation Failure Mode

The shock-flame decoupling mode for case (iii), $\alpha = 15°$, is shown in Fig.5, where the detonation wave decays to the shock followed by the reaction zone behind it after the Mach reflection. Under this condition, the detonation wave first shows more significant attenuation in the expansion region of the obstacle. At $t = 0.846$ ms, the incident shocks collide at the trailing edge of the obstacle, where the Mach reflection occurs. The Mach stem continuously evolves to the leading shock front with a certain curvature. The flame surface always lags behind the leading shock, demonstrating the decoupling of shock and flame. In Fig.5 (e), it can be seen that the inert transverse shocks propagate along the induction zone behind the slip line. The heated gas accumulates

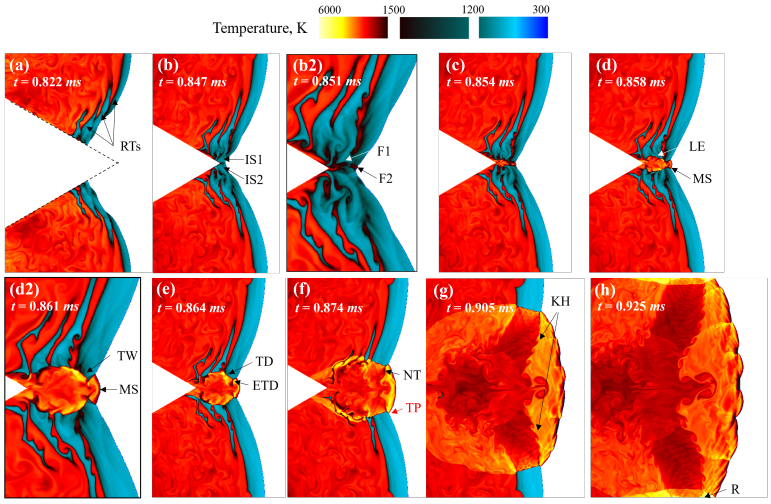

Fig. 4: Temperature fields of detonation reinitiation mode of different time steps. The y axis is the full span of the setup channel, except for (b2) and (d2) figures in black frame that are zoomed in for more details. (RTs: reaction tongues, IS: shock wave, F: ignition kernel, LE: local explosion, MS: Mach stem, TW: transverse wave, TD: transverse detonation, ETD: extended transverse detonation, KH: Kelvin-Helmholtz instability, NT: non-reactive tail, R: reflection.)

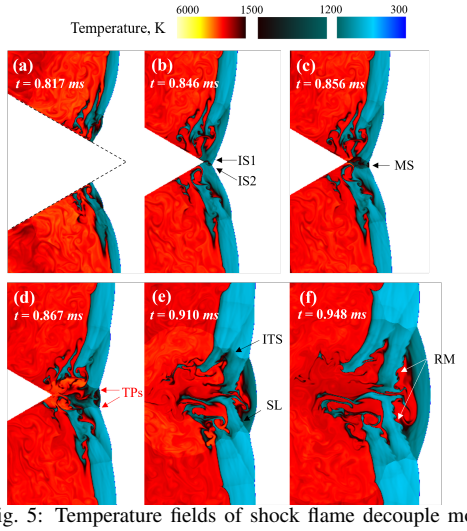

Fig. 5: Temperature fields of shock flame decouple mode at different time steps. (IS: shock wave, MS: Mach stem, SL: slip line, ITS: inert transverse shock, RM: Richtmyer–Meshkov instability)

in the form of jet flow behind the Mach shock over time in the presence of Richtmyer–Meshkov instabilities. Although this instability promotes the interaction of the turbulent flame with the Mach shock induced zone, the detonation in this case decays to a failure mode with no reinitiation. This differs from previous experiments involving hydrocarbon-oxygen detonations, such as stoichiometric mixtures of CH_4, C_2H_4, C_2H_6, and C_3H_8. These mixtures have been observed to re-amplify after traveling significant distances beyond obstacles, with the turbulent reaction zone structure remaining closely coupled to the leading shock due to relatively smaller cell size and lower chemical sensitivity than hydrogen mixtures. For hydrocarbons, it is suggested that the formation of strong jets behind periodically formed Mach shocks provides localized enhancement of reactivity through turbulent mixing [22–24].

By increasing α to 20°, the detonation propagation mode changes to an inert shock without ignition behind the Mach reflection, as shown in Fig.6. The decoupling of the shock front and flame is more pronounced in the expansion region of the obstacle. At the trailing edge of the obstacle, two incident shocks interact with each other, forming an inert Mach wave. Due to the long decoupling distance between the shock and the flame, there is no re-ignition event behind the Mach shock in the propagation process. At $t = 0.993$ ms, the double triple points configuration becomes apparent in Fig.6 (e), and eventually merges as the shock wave propagates downstream.

3.3. Critical Conditions with $D(\kappa)$ Curve

The previous sections have presented various detonation propagation modes, including reinitiation mode, shock-flame decoupling mode, and fully quenched mode. In the following sections, we provide a theoretical analysis for determining the critical conditions among these modes. First, the asymptotic theory of self-sustained detonation within the Detonation Shock Dynamics (DSD) framework [11] is introduced. Here, a virtual sonic locus is defined as the location where the Mach number in shock-attached frame equals the sonic speed. For a self-sustaining detonation, the shock speed must always exceed the local sonic speed behind the shock. Therefore, the sonic locus is crucial for determining whether the detonation wave can propagate stably. If the shock front

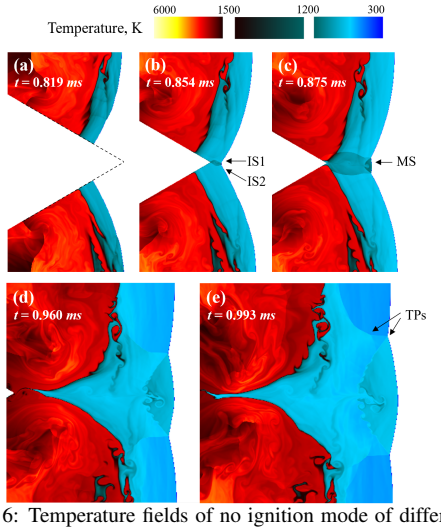

Fig. 6: Temperature fields of no ignition mode of different time steps. (IS: shock wave, MS: Mach stem, TPs: triple points.)

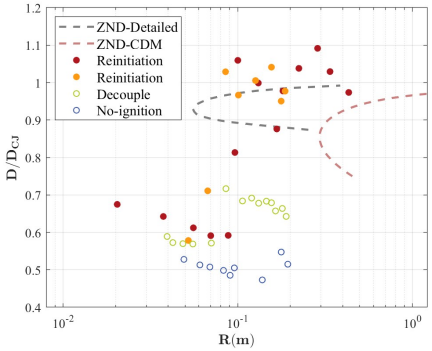

Fig. 7: The nondimensional detonation speed versus shock front curvature and predictions derived from the Generalized ZND model.

decelerates and reaches a subsonic speed, detonation failure occurs and detonation degrades to deflagration.

The analysis reveals the intrinsic relationship in shock speed, shock acceleration, and the shock front curvature ($\dot{D} = a_1\dot{\omega} - a_2\kappa$ where $\dot{\omega}$ is reaction rate and κ is shock front curvature). Heat release from chemical reaction gives positive effects to the shock acceleration, while the dissipation from curved expansion gives negative effects. Two competing mechanisms finally reach a balanced state during the detonation propagation.

In order to get the relationship between detonation speed and the shock front curvature from the generalized ZND model, we solve the equations (details in appendix) on the framework of *Cantera*, and *Shock and Detonation Toolbox*. A detailed reaction mechanism *San Diego* and a one-step mechanism from CDM are both adopted for the analysis of hydrogen-air mixture combustion at 1 atm.

Fig.7 shows the simulated results of different detonation modes (2 detonation reinitiation cases and 2 detonation failure cases) compared against the ZND solution using both detailed chemistry and CDM. The x axis is the curvature radius ($R = 1/\kappa$) and the y axis is the nondimensional velocity measured on the centerline of the channel after Mach reflection. The shock front curvature is obtained by means of image processing and fitting from SciPy. For the two detonation reinitiation cases, corresponding to case (i) and (ii) in Fig.2, the velocity is relatively low at the early stage after Mach reflection, and then undergoes a sharp increase indicating successful detonation reinitiation. After reaching the top of the curve, the velocity gradually relaxes towards the CJ speed in an oscillatory manner. In contrast, for the two detonation failure modes, the velocity decreases oscillatory as the curvature radius increases, and it will never reach the lower branch of ZND curve. This indicates that the detonation attenuates to shock-flame decoupling state or even inert Mach shock with no ignition, and reinitiation will not occur under these circumstances. For the decoupling case, despite the fact that we find some promotion mechanisms in the temperature fields, the detonation cannot be reinitiated and sustained. This is because the heat release due to chemical reaction, which represents the primary factor for acceleration, cannot balance the negative effects of diffusion. Moreover, the absolute nondimensional velocity of no-ignition mode is smaller than that of shock-flame decoupling, which means the detonation attenuation is more significant in this case. Note that in Fig.7, the theoretical curve using detailed chemistry is positioned on the left side to the curve using CDM. The critical κ for the detailed mechanism is $\kappa_{\text{detailed}} = 17.857\ \text{m}^{-1}$, and the critical κ for the CDM is $\kappa_{\text{CDM}} = 3.390\ \text{m}^{-1}$. Using a symmetric relative error definition, the difference is about $|\kappa_{\text{detailed}} - \kappa_{\text{CDM}}| * 2/(\kappa_{\text{detailed}} + \kappa_{\text{CDM}}) = 136\%$. This shift arises from the inherent characteristics of the CDM model being used. In a single step model, the thermicity distribution closely overlaps with the reaction zone, as heat release increases exponentially with temperature and no distinct induction zone is present. The relatively lower peak thermicity from the one-step chemistry leads to a lower critical curvature and a reduced ability of the detonation to overcome dissipation from curved expansion. Nevertheless, the theoretical ZND curve using the current CDM provides a more reliable prediction of the critical conditions for detonation reinitiation.

From these results, it is concluded that the transition between detonation formation and ignition is strongly correlated with the critical curvature. This agrees well with the curvature concept proposed by Kasimov and Stewart [11] for quasi-steady curved detonations. It is worth noting here that Xiao et al. [21] previously experimentally examined the similar

diffusive phenomena of gaseous detonations in the channel with exponentially enlarging cross-sections, which confined the detonation lateral strain and so that the velocity curvature follows better with the theoretical D(κ) curve compared with our numerical results. For the cases in this study, the Mach shock is not constrained by the channel from emergence to the detonation reinitiation, and thus the velocity may oscillate around the theoretical curve which is consistent with previous experimental results [12]. Nevertheless, it is significant in our study confirming that the critical curvature for weakly-curved detonations in the regular structure hydrogen–air mixture can be well predicted by the laminar ZND theory. Thus the use of such criteria can serve as a starting point for the design of numerical simulations.

3.4. Critical Conditions with Critical Decay Rate Model

The above $D(K)$ theory can identify between successful detonation reinitiation and failure; however, it does not distinguish the specific nature of the failure mode (shock-flame decoupling or complete quenching). Therfore, the critical decay rate (CDR) model is being applied. CDR attributes the extinction of the ignition mainly to the rapid gas dynamic expansion behind the decaying shock, which is particularly relevant for configurations involving diverging geometries or shock reflections, where the leading shock undergoes deceleration process [25]. A dimensionless ignition parameter that captures the competition between chemical induction and flow expansion along a particle path can thus predict the failure of ignition:

$$\zeta = \frac{E_a}{RT_{vn}}(\gamma - 1)\frac{t_i}{t_{exp}} \tag{1}$$

where $E_a/(RT_{vn})$ is the reduced activation energy, t_i is the ignition delay time, which is calculated from Cantera, and t_{exp} is the characteristic time of explosion along the particle path. If ζ remains below unity, indicating that the chemical reaction rate could overcome the expansion effect, the ignition state can be maintained. Conversely, when ζ exceeds the critical value, the expansion effect dominates behind the shock and in the case quenching event will occur.

To apply this criterion in realistic shock environments, particularly where the shock front is both decelerating and curved, Radulescu extended the model from Eckett with the shock change relations and fluid particle tracking in the post-shock frame [12], and the expansion rate was reformulated as:

$$t_{exp}^{-1} = \frac{1}{\rho}\frac{D\rho}{Dt} = \frac{6}{\gamma+1}\frac{\dot{D}}{D} + \frac{2D\kappa(\gamma-1)}{(\gamma+1)^2} \tag{2}$$

where $\dot{D}/D = dD/dx$ is deceleration divided by shock speed, which is obtained from simulation probe on the horizontal center-line of shock front, and κ is curvature of shock front extracted by fitting the instantaneous shock front. The first term represents the effect of shock decaying, and the second term accounts for the contribution of local expansion.

Comparing this analytical criterion with the simulation results, the shock decay rate is plotted in Fig.8. The computed values of the decay rate (ζ) from different cases clearly separate the ignition(both reinitiation and decoupled modes) and fully quenched modes. This result is consistent with the concept that the ignition process is not only by achieving a sufficient temperature behind the shock, but is fundamentally governed by the energy release time relative to the shock decaying time.

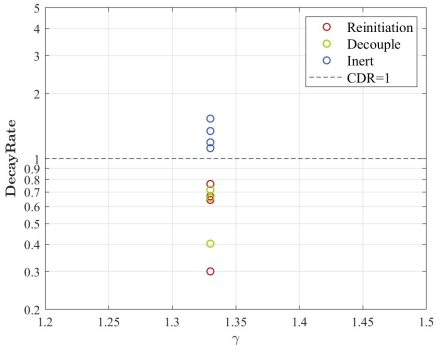

Fig. 8: The decay rate of hydrogen-air mixture versus specific heat ratio. The dashed line is critical decay rate $\zeta = 1$.

While this model accurately predicts the transition between ignition and non-ignition, it does not fully capture the threshold separating decoupling mode (deflagration) from detonation reinitiation. For some relatively weak ignition events, the flame can be sustained behind the shock wave, but the acceleration cannot catch up with the shock front to form coupling, such a decoupled shock-flame phenomenon will appear instead of a self-sustaining propagating detonation.

4. Summary and Conclusions

The detonation attenuation and reinitiation process in an obstructed channel filled with stoichiometric hydrogen-air mixture is studied through high-fidelity simulations with a calibrated chemical diffusive model (CDM). A diamond-shaped obstacle is placed in the channel to generate a Mach reflection process. Three different detonation propagation modes behind the obstacle are captured: detonation reinitiation mode, shock flame decoupling mode, and fully quenched mode, all of which show good agreement with an earlier experiment. The ignition dynamics after the Mach reflection is further analyzed. The detonation reinitiaion mode is characterized by transverse detonation waves that emerge shortly after Mach reflection and rapidly re-establish a self-sustained detonation. In the shock-flame decoupling mode, turbulent reaction zone decouples with the shock wave, and the turbulent mixing fails to trigger a detonation ignition. For the fully quenched mode, inert Mach shock forms with no-ignition.

To identify the critical conditions separating these modes, two theoretical frameworks are employed. The first framework is based on the quasi-steady one-dimensional $D(\kappa)$ relationship using the generalized ZND models for hydrogen-air mixtures, which accurately envelops the detonation reinitiation region when compared to the simulated results. The second framework, the critical decay rate model, focuses on the ignition delay time versus shock decaying characteristic time, providing a clear criterion distinguishing ignition from fully quenched mode. These results further confirm the validity of theoretical models in predicting detonation behaviors in hydrogen-air mixtures, offering a possible solution or approach for detonation ignition diagnostics in practical contexts.

Declaration of Competing Interest

The authors declare that they have no known competing financial interests or personal relationships that could have appeared to influence the work reported in this paper.

Acknowledgments

This study was supported by the National Science Foundation of China (Grant No. 12572417), the Natural Sciences and Engineering Research Council of Canada (Grant No. RGPIN-2023-03309) and Alberta Innovates. We also would like to acknowledge Dr. Farzane Zangene from University of Ottawa for the discussion on DSD theoretical framework development and the suggestion of using critical decay rate model by Prof. Remy Mevel.

Supplementary Material

Supplemental material with regard to the simulation model (S1), grid resolution test (S2), and detonation velocity distributions (S3) are included.

References

[1] B. M. Maxwell, R. R. Bhattacharjee, S. S. M. Lau-Chapdelaine, S. A. E. G. Falle, G. J. Sharpe, M. I. Radulescu, Influence of turbulent fluctuations on detonation propagation, Journal of Fluid Mechanics 818 (2017) 646–696.

[2] R. Bhattacharjee, S. Lau-Chapdelaine, G. Maines, L. Maley, M. Radulescu, Detonation re-initiation mechanism following the Mach reflection of a quenched detonation, Proc. Combust. Inst. 34 (2) (2013) 1893–1901.

[3] S. Tang, S. Zhang, S. Lai, X. Fang, Effect of activation energy on detonation cellular dynamics and reinitiation behaviors, AIAA Journal 63 (5) (2025) 1778–1788.

[4] Y. Fortin, J. Liu, J. H. Lee, Mach reflection of cellular detonations, Combust. Flame 162 (3) (2015) 819–824.

[5] Z. Yang, B. Zhang, H. D. Ng, Experimental observations of gaseous cellular detonation reflection, Proc. Combust. Inst. 40 (1) (2024) 105519.

[6] D. Jun, D. Kwon, B. J. Lee, Numerical study on the reinitiation mechanism of detonation propagating through double slits in a planar channel, Combust. Flame 261 (2024) 113271.

[7] G. Rainsford, D. J. S. Aulakh, G. Ciccarelli, Visualization of detonation propagation in a round tube equipped with repeating orifice plates, Combust. Flame 198 (2018) 205–221.

[8] D. Tropin, K. Vyshegorodcev, Numerical simulation of interaction of cellular detonation wave with systems of inert porous filters, International Journal of Hydrogen Energy 48 (48) (2023) 18454–18485.

[9] X. Jia, Y. Xu, H. Zheng, H. Zhang, Direct detonation initiation in hydrogen/air mixture: effects of compositional gradient and hotspot condition, Journal of Fluid Mechanics 970 (2023) A22.

[10] S. S.-M. Lau-Chapdelaine, M. I. Radulescu, Viscous solution of the triple-shock reflection problem, Shock Waves 26 (5) (2016) 551–560.

[11] A. R. Kasimov, D. S. Stewart, Asymptotic theory of evolution and failure of self-sustained detonations, Journal of Fluid Mechanics 525 (2005) 161–192.

[12] F. Zangene, M. I. Radulescu, The critical conditions for the re-ignition and detonation formation from Mach reflections of curved decaying shocks, Proc. Combust. Inst. 40 (1-4) (2024) 105774.

[13] C. A. Eckett, J. J. Quirk, J. E. Shepherd, The role of unsteadiness in direct initiation of gaseous detonations, Journal of Fluid Mechanics 421 (2000) 147–183.

[14] X. Lu, C. R. Kaplan, E. S. Oran, Calibrating the chemical-diffusive model using the detonation cell data, in: AIAA Scitech 2021 Forum, American Institute of Aeronautics and Astronautics, 2021.

[15] S. Lai, S. Tang, C. Xu, N. Sekularac, X. Fang, Computational diagnostics for flame acceleration and transition to detonation in a hydrogen/air mixture, Combust. Flame 258 (2023) 113054.

[16] H. Xiao, E. S. Oran, Shock focusing and detonation initiation at a flame front, Combust. Flame 203 (2019) 397–406.

[17] X. Lu, C. R. Kaplan, E. S. Oran, A chemical-diffusive model for simulating detonative combustion with constrained detonation cell sizes, Combust. Flame 230 (2021) 111417.

[18] J. M. Austin, The role of instability in gaseous detonation, Ph.D. thesis, California Institute of Technology (2003).

[19] G. Floring, M. Peswani, B. Maxwell, On the role of transverse detonation waves in the re-establishment of attenuated detonations in methane–oxygen, Combust. Flame 247 (2023)

112497.
[20] V. Gamezo, A. Vasil'ev, A. Khokhlov, E. Oran, Fine cellular structures produced by marginal detonations, Proc. Combust. Inst. 28 (1) (2000) 611–617.
[21] Q. Xiao, M. I. Radulescu, Dynamics of hydrogen–oxygen–argon cellular detonations with a constant mean lateral strain rate, Combust. Flame 215 (2020) 437–457.
[22] B. Maxwell, A. Pekalski, M. Radulescu, Modelling of the transition of a turbulent shock-flame complex to detonation using the linear eddy model, Combust. Flame 192 (2018) 340–357.
[23] Z. Huang, H. Zhang, Ignition and deflagration-to-detonation transition modes in ethylene/air mixtures behind a reflected shock, Physics of Fluids 34 (8) (2022) 086105.
[24] M. A. Adigüzel, R. Küçükosman, A. A. Yontar, P. Roy, D. Üstün, Y.-T. Chen, Turbulence-driven shock wave enhancement in detonation engines through obstacle design across hydrogen, acetylene, and kerosene, Physics of Fluids 37 (8) (2025) 086162.
[25] Y. Tan, R. Mével, Y. C. Liu, A review on ignition in expanding gaseous media, Process Safety and Environmental Protection 179 (2023) 241–256.

Appendix

S1: Details on Governing Equations and CDM Parameters

The simulations presented in this study solve the unsteady fully-compressible Navier-Stokes equations coupled with a single-step chemical diffusive model (CDM). The governing equations describing the conservation of mass, momentum, energy, and species read:

$$\frac{\partial \rho}{\partial t} + \nabla \cdot (\rho \boldsymbol{U}) = 0, \tag{A1}$$

$$\frac{\partial \rho \boldsymbol{U}}{\partial t} + \nabla \cdot (\rho \boldsymbol{U}\boldsymbol{U}) + \nabla p = \nabla \cdot \hat{\boldsymbol{\tau}}, \tag{A2}$$

$$\frac{\partial (\rho E)}{\partial t} + \nabla \cdot ((\rho E + p)\boldsymbol{U}) = \nabla \cdot (\boldsymbol{U} \cdot \hat{\boldsymbol{\tau}}) + \nabla \cdot (K \nabla T) - \rho q \dot{w}, \tag{A3}$$

$$\frac{\partial \rho Y}{\partial t} + \nabla \cdot (\rho Y \boldsymbol{U}) + \nabla \cdot (\rho D \nabla Y) = \rho \dot{w}, \tag{A4}$$

where ρ, $\boldsymbol{U}$, p, and T represent the density, velocity, pressure, and temperature of the gas. E is the specific total energy, $\dot{w}$ is the chemical reaction rate, q is the chemical energy release, Y is the mass fraction of the reactant, K is the thermal conductivity, and D is the mass diffusivity.

The gas follows the ideal gas equation of state,

$$p = \frac{\rho R T}{M}, \tag{A5}$$

where R is the universal gas constant, and M is the molecular weight.

The viscous stress tensor is defined as

$$\hat{\tau} = \rho \nu ((\nabla \mathrm{U}) - (\nabla \mathrm{U})^T - \frac{2}{3}((\nabla \cdot \mathrm{U})\mathrm{I}), \tag{A6}$$

where ν is the kinematic viscosity, I is the unit tensor, and the superscript T denotes the matrix transposition. The specific total energy E is calculated by

$$E = \frac{p}{(\gamma - 1)\rho} + \frac{1}{2}(\boldsymbol{U} \cdot \boldsymbol{U}), \tag{A7}$$

where γ is the specific heat ratio.

As stated in the main article, the premixed stoichiometric combustion of hydrogen-air mixture is studied using a calibrated, one-step chemical-diffusive model (CDM) where the reaction rate follows a first-order Arrhenius equation:

$$\dot{\omega} = dY/dt = -A\rho Y \exp(-E_a/RT) \tag{A8}$$

where A and E_a represent the pre-exponential factor and the activation energy, respectively. In this model, it is assumed that the kinematic viscosity, diffusion, and heat conduction all depend on the temperature in a comparable way:

$$\nu = \nu_0 \frac{T^{0.7}}{\rho}, \quad D = D_0 \frac{T^{0.7}}{\rho}, \quad \frac{K}{\rho C_\mathrm{p}} = \kappa_0 \frac{T^{0.7}}{\rho} \tag{A9}$$

The diffusive processes of CDM are characterized by transport constants. The interrelationship among ν_0, D_0, and κ_0 is elucidated through three dimensionless parameters: Lewis, Prandtl, and Schmidt numbers:

$$\mathrm{Le} = \frac{K}{\rho C_\mathrm{p} D} = \frac{\kappa_0}{D_0}, \quad \mathrm{Pr} = \frac{\rho C_\mathrm{p} \nu}{K} = \frac{\nu_0}{\kappa_0}, \mathrm{Sc} = \frac{\nu}{D} = \frac{\nu_0}{D_0} \tag{A10}$$

A calibrated, single-step, chemical-diffusive model (CDM) is used to study the stoichiometric hydrogen-air mixture. The CDM parameters typically used to study the DDT process are calibrated such that the combustion in both flame and detonation regimes can be accurately captured [16]. Considering the physical phenomenon of detonation reinitiation presented in this paper, however, the detonation wave properties has a more predominant role compared with the laminar flame properties. Therefore, a calibrated set of parameters using a recently developed optimization procedure by Lu et al.[14] with specific emphasis on detonation cell size is used, and the detailed thermo-chemical parameters are provided in Table A1.

Table A1: Input model parameters and output combustion wave properties for stoichiometric premixed hydrogen-air mixture initially at 1 atm and 298 K.

Parameters	Descriptions	Value
	Input Parameters	
γ	Adiabatic index	1.33
M	Molecular weight	27 g/mol
A	Pre-exponential factor	4.55×10^{9} cm^3/(g s)
E_a	Activation energy	38.5 RT_0
q	Chemical energy release	26.33 RT_0/M
ν_0	Viscosity	2.54×10^{-5} g/(s cm K$^{0.7}$)
$\kappa_0 = D_0$	Transport constants	2.54×10^{-5} (g/s cm K$^{0.7}$)
	Output Properties	
$\mathcal{E}$	Effective activation energy	6 RT_{vn}
$\chi_{\rm d}$	Half-reaction thickness	0.17 cm
$D_{\rm CJ}$	CJ detonation velocity	2000 m/s
λ	Detonation cell size	$\sim$ 6 cm

S2: Grid Resolution Test

All simulations presented in this work use a uniform grid size with a cell size $dx = 100$ μm. Figure A1 shows the cellular structures with three different grid sizes: 200, 100, and 50 μm. The detonation wave structures are found consistent to each other, only in case of $dx = 50$ μm, some of the cells bifurcate into multiple smaller cells, indicating secondary cell structures. A quantitative evaluation of detonation cell size is further given by the auto-correlation function (ACF). The detonation cell sizes for dx =200, 100, and 50 μm are 4.86, 5.04, and 4.64 cm, respectively. And the ACF correlation results also support the grid convergence, for more details in our recent work[3]. Since the current study is not focused on secondary cell structures, $dx = 100$ μm is adopted as it adequately the key flame properties for detonation propagation, reinitiation, and decoupling.

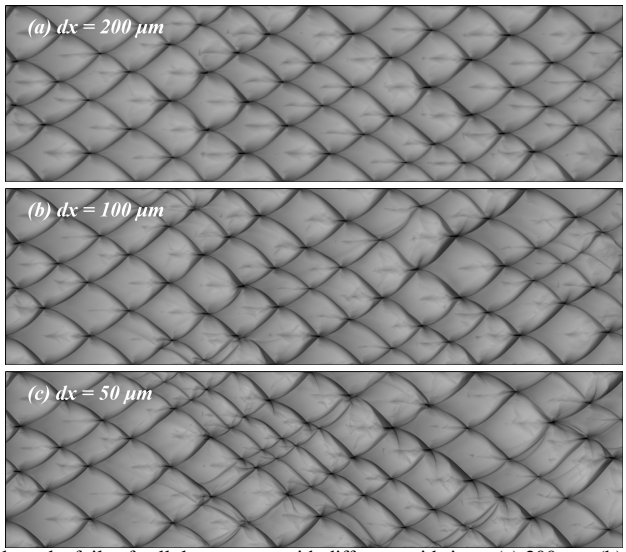

Fig. A1: Numerical smoke foils of cellular patterns with different grid sizes: (a) 200μm; (b) 100μm; (c) 50μm.

S3: Shock Velocity Distributions of Different Propagation Modes

Figure A2 shows the detonation velocity evolution from decaying process to the Mach shock reestablishment. The velocities of the incident shock in the expansion region of the obstacle are measured along the channel top wall and the velocities of the Mach shock are measured along the center line. A significant deceleration of the local velocity profile along the expansion region occurs, with the velocity decreasing to 0.6-0.7D_{CJ} for all the cases. After the interaction of the two decaying shocks, the compression effect and reinitiation process take a period of time and form a new Mach shock. For the detonation reinitiation case, the shock speed rapidly increases to nearly CJ speed and then oscillates near the CJ speed. For the shock-flame decouple mode, the detonation velocity increases to about 0.7D_{CJ} after Mach reflection and then decelerates as the unburned gas accumulates behind the shock front. For the no-ignition mode, the shock velocity remains below 0.6D_{CJ} after reflection and continues to decay as the formation of inert shock.

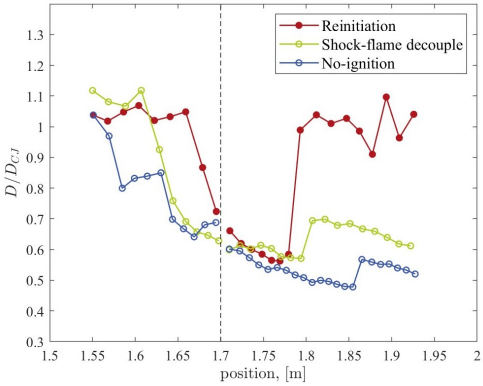

Fig. A2: Detonation velocity evolution along x axis positions, dashed line represents the trailing edge of the obstacle (1.7 m).

S4: Details on Theoretical D(k) Curve Solutions

For the quasi-steady (acceleration $\dot{D}$ equals to 0) one-dimensional reacting flow behind the curved shock front of the detonation wave, the governing equations in the shock-attached frame can be expressed as a set of ordinary differential equations (ODEs) [21]:

$$\frac{dp}{dt} = -\rho u^2 \frac{\dot{\sigma}_{re} - \dot{\sigma}_A}{1 - M^2} \tag{A11}$$

$$\frac{d\rho}{dt} = -\rho \frac{\dot{\sigma}_{re} - M^2 \dot{\sigma}_A}{1 - M^2} \tag{A12}$$

$$\frac{du}{dt} = u \frac{\dot{\sigma}_{re} - \dot{\sigma}_A}{1 - M^2} \tag{A13}$$

$$\frac{dy}{dt} = \frac{W_i \dot{w}_i}{\rho}, \quad (i = 1, ..., N_s) \tag{A14}$$

$$\dot{\sigma}_{re} = \sum_{i=1}^{N_s} \left(\frac{W}{W_i} - \frac{h_i}{C_p T}\right) \frac{dy_i}{dt} \tag{A15}$$

$$\dot{\sigma}_A = K(D_s - u) \tag{A16}$$

where ρ, p, M, C_p, h_i, y_i, W_i, $\dot{w}_i$, and N_s are the mixture density, pressure, local Mach number ($M = u/c$), specific heat at constant pressure, enthalpy of species i, species mass fraction, molecular weight of species i, molar production rate of species i, and the total number of species. u is the velocity in shock-attached frame, which means $u = v - D_s$ where v is the normal velocity in lab frame and D_s is the detonation shock velocity. $\dot{\sigma}_{re}$ is the thermicity, $\dot{\sigma}_A$ is the rate of lateral strain, and κ is the curvature of the detonation front. The thermicity represents heat release from chemical reaction which accelerates the gas to transonic and supersonic states, while the lateral strain from diffraction plays a role of deceleration. The ODEs system's singular point at $M = 1$ ($u = c$) means the gas reaches sonic locus, and at this locus $\dot{\sigma}_{re}$ and $\dot{\sigma}_A$ reach a balance state, which names generalized CJ condition.